*Korean J. Chem. Eng.*, 37(5), 891-897 (2020)
DOI: 10.1007/s11814-020-0496-3

pISSN: 0256-1115
eISSN: 1975-7220

# Solvo-hydrothermal synthesis of calcium phosphate nanostructures from calcium inositol hexakisphosphate precursor in water-ethanol mixed solutions

**Ji-Hoon Han*, Seung Pil Pack**, and Sungwook Chung*,†**

*School of Chemical and Biomolecular Engineering, Pusan National University,
2 Busandaehak-ro 63beon-gil, Geumjeong-gu, Busan 46241, Korea
**Department of Biotechnology and Bioinformatics, Korea University, 2511 Sejong-ro, Sejong 30019, Korea
(*Received 30 September 2019 • accepted 18 January 2020*)

**Abstract**−We report the synthesis and characterization of crystalline calcium phosphate (CaP) nanostructures from calcium inositol hexakisphosphate ($CaIP_6$) precursor in water-ethanol mixed solutions. We show how these CaPs can be prepared by a solvo-hydrothermal reaction and determined their compositions and structures using a battery of material characterization techniques. Our results show that only the hydroxyapatite (HAP) and dicalcium phosphate anhydrous (DCPA) phases of CaP were present in the nanostructures produced in water-ethanol mixtures, and that HAP/DCPA ratio of the rod- and plate-shaped CaP nanostructures produced were affected by the amount of ethanol present in these mixtures. The described method can be used to improve morphological control of CaP-based biomaterials and has potential use in bone regenerative medicine.

Keywords: Solvo-hydrothermal Synthesis, Calcium Phosphate, Nanostructures, Hydroxyapatite, Dicalcium Phosphate Anhydrous

## INTRODUCTION

Calcium phosphates (CaPs) are important in the tissue engineering, regenerative medicine, and drug delivery fields due to their excellent biocompatibility, low toxicity, and outstanding osteoconductivity [1-4]. CaP-based materials have many potential uses in biomedical applications due to their unique bioactivity, biocompatibility, and mechanical properties, and are used as scaffold materials for bone and tooth repair [2,5,6], bioactive coatings and fillers [7,8], composite materials [9], and drug delivery transporters [10-12]. These material properties strongly depend on CaP morphology, crystallinity, composition, and particle size [13], and thus, the ability to control CaP morphology, crystallinity, composition, and size (typically, with lengths in the nanometer to sub-micron range) is of great importance for their applications.

CaPs with different phases have been synthesized in numerous ways [14-17] and the majority of them have been based on the use of hydroxyapatite (HAP, $Ca_{10}(PO_4)_6(OH)_2$), because it is one of the key mineral components of the bones and teeth of vertebrate [1]. Some excellent reviews have been published on the advances made in the syntheses of CaP crystals with various sizes and shapes [14,18,19]. HAP is commonly used as bone graft and filler [2], and as drug delivery carrier [10-12], catalyst [20], and adsorbent [17]. Monetite (dicalcium phosphate anhydrous (DCPA, $CaHPO_4$)), has also been used for bone regeneration applications because it is absorbed more rapidly than HAP *in vivo*, and thus better promotes bone regeneration [21]. DCPA is also used commercially to produce bone cements, toothpastes, and food additives [22], and as a precursor material to produce HAP [16]. For these reasons, HAP- and DCPA-based composites represent promising alternatives to conventional implant replacement materials.

Phytic acid (inositol hexakisphosphate ($IP_6$)), is a non-toxic six-

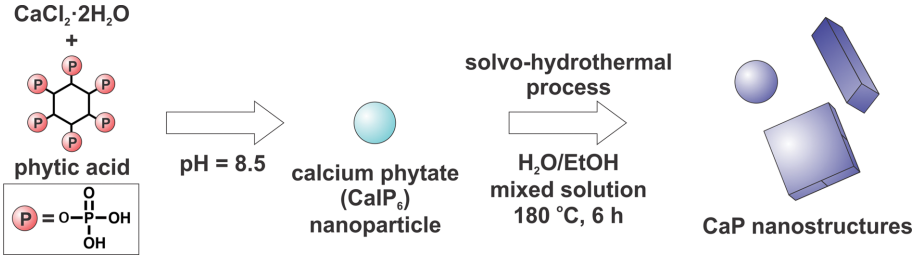



**Fig. 1. Schematic diagram of the preparation of CaP nanostructures from $CaIP_6$ precursor nanoparticles in the water-ethanol mixtures under solvo-hydrothermal conditions.**

†To whom correspondence should be addressed.
E-mail: sungwook.chung@pusan.ac.kr
Copyright by The Korean Institute of Chemical Engineers.

fold dihydrogenphosphate ester of inositol typically found in mammalian cells and plant tissues [23]. $IP_6$ contains six phosphate groups attached to a six-membered carbocyclic sugar. At physiological pH conditions, these phosphates are partially ionized so that they become negatively charged. These charges offer a high binding affinity to metal ions such as $Ca^{2+}$ and $Mg^{2+}$. $IP_6$ is also used to protect teeth because it prevents the dissolution of crystalline HAP from tooth enamel [24], and recent studies have revealed $IP_6$ is involved in the inhibition of pathological calcification in soft tissues [23]. Grases et al. reported $IP_6$ suppressed the crystallization of CaP from solution under ambient conditions [25]. Although the detailed mechanisms are not fully understood, $IP_6$ is believed to inhibit the crystal growth by adsorbed onto HAP nuclei or certain crystalline facets of HAP, which suggests $IP_6$ may play an important role in affecting the growth of CaP crystals under physiological conditions. However, few studies have investigated the effect of $IP_6$ on CaP crystal growth under hydrothermal conditions, which usually involves relatively high temperatures and pressures [23,26].

Herein, we present a means of synthesizing crystalline CaP nanostructures with different phases from $CaIP_6$ nanoparticles under solvo-hydrothermal conditions and describe the influence of water-ethanol solution compositions on the crystalline phases, morphologies, and sizes of the CaP nanostructures produced.

## EXPERIMENTAL SECTION

### 1. Materials

Calcium chloride dihydrate ($CaCl_2{\cdot}2H_2O$, 98%), sodium hydroxide (NaOH), and ethanol ($CH_3CH_2OH$, 99.9%) were obtained from Daejung Chemical & Metals Co. (Korea), Ltd. An aqueous solution of *myo*-inositol hexakis(dihydrogen phosphate) ($C_6H_{18}O_{24}P_6$, 50% (w/w)) was purchased from Sigma-Aldrich (USA). All other chemicals were of analytical ACS Regent grade and once purchased they were used without further purification.

### 2. Preparation of Calcium Inositol Hexakisphosphate ($CaIP_6$) Precursor

$CaIP_6$ nanoparticles were synthesized as previously described with a few modifications [27]. 2.20 g (1.67 mmol) of a 50% (w/w) aqueous solution *myo*-inositol hexakis(dihydrogen phosphate) and 1.47 g (10 mmol) of $CaCl_2{\cdot}2H_2O$ were added to 400 mL of 18.2 MΩ ultrapure water (Milli-Q purification system, Millipore Corporation) at room temperature and a Ca to P atomic ratio of 1 : 1. The pH of the solution was adjusted to ~8.5 with 1 N sodium hydroxide (NaOH) solution while vigorously stirring at 300 rpm for 1.5 hr. The solution turned from a clear light brown to an opaque white during the reaction. After reaction completion, the mixture was centrifuged at 18,686 ×g for 10 min, filtered through a mixed cellulose ester membrane of a pore diameter of 0.45 μm, rinsed with an excess of deionized water followed by absolute ethanol, re-dispersed in deionized water, centrifuged at 18,686 ×g for 25 min, and filtered. The resulting white product was dried in a vacuum oven at 90 °C to give ~1.48 g (~17% yield) of $CaIP_6$ nanoparticles. Finally, the $CaIP_6$ nanoparticles were stored in a desiccator at ~4 °C.

### 3. Preparation of CaP Nanostructures via a Solvo-hydrothermal Reaction of $CaIP_6$ Precursor in Water-ethanol Mixed Solutions

CaP nanostructures were synthesized from $CaIP_6$ precursor under

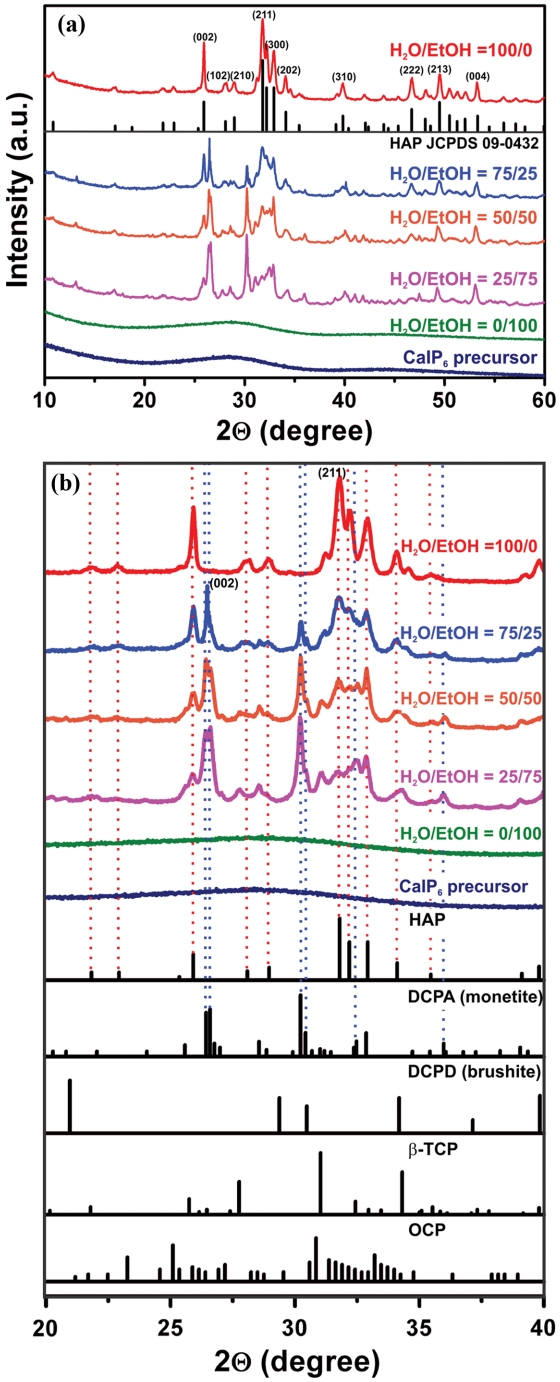



**Fig. 2. (a) Survey XRD patterns of as-synthesized CaP nanostructures synthesized in water-ethanol mixture $H_2O$/EtOH (v/v %)= 100/0, 75/25, 50/50, 25/75, and 0/100. (b) Comparison of the XRD patterns of CaP nanostructures synthesized in water-ethanol mixtures ($H_2O$/EtOH (v/v %)=100/0, 75/25, 50/50, 25/75, and 0/100) and standard XRD patterns of the hydroxyapatite (HAP) (JCPDS No. 09-0432, ICDD 98-000-1706), dicalcium phosphate anhydrous (DCPA or monetite) (JCPDS No. 09-0080, ICDD 01-071-1795), dicalcium phosphate dihydrate (DCPD or brushite) (JCPDS No. 09-0077, ICDD 98-017-2261), $\beta$-tricalcium phosphate ($\beta$-TCP) (JCPDS No. 09-0169, ICDD 01-070-2065), and octacalcium phosphate (OCP) (JCPDS No. 26-1065, ICDD 98-006-5347) phases of CaP. Dotted lines indicate peak assignments.**

solvo-hydrothermal conditions (Fig. 1). In a typical experiment, ~110 mg of $CaIP_6$ nanoparticles were added to ~40 mL mixture of ethanol and 18.2 MΩ ultrapure water, at v/v % ratio of 100/0, 75/25, 50/50, 25/75, and 0/100, and ultrasonicated at room temperature to produce clear solutions. Then, the resulting solutions were transferred to a 100 mL Teflon-lined stainless steel autoclave and heated at ~180 °C for ~6 hr. After cooling to room temperature, the solutions were then filtered through a Nylon membrane of pore diameter of 0.2 μm. The resulting white powders were washed with an excess of deionized water and absolute ethanol and dried in air at room temperature. The weights of final products for water/ethanol compositions of 100/0, 75/25, 50/50, 25/75, and 0/100 were ~43 mg (yield ~35%), ~46 mg (~41%), ~58 mg (~56%), ~68 mg (~64%), and ~99 mg (~90%), respectively.

**4. Characterization**

X-ray powder diffraction (XRD) patterns were obtained using a Philips X'Pert-MPD diffractometer with a monochromatized source of Cu $K_{\alpha 1}$ radiation ($\lambda$=0.15405 nm) at 1.6 kW power (40 kV, 30 mA). Fourier transformation infrared spectroscopy (FT-IR) was performed on a Spectrum GX FT-IR spectrometer. The morphology of CaP nanostructures was determined by field emission scanning electron microscopy (FESEM) using a Zeiss Supra 40 FESEM microscope at an accelerating voltage of 5 to 10 kV and by transmission electron microscopy (TEM) using a Hitachi H-7600 TEM unit operating at an accelerating voltage of 80 kV. High-resolution TEM (HRTEM) analysis was performed using an FEI TALOS F200X unit at an operating at accelerating voltage of 200 kV.

## RESULTS AND DISCUSSION

Fig. 2 shows the XRD patterns of as-synthesized CaP products synthesized using the solvent mixtures shown in Table 1. The XRD pattern of the reaction product obtained using 100% ethanol (olive curve, Fig. 2) closely resembled that of the amorphous $CaIP_6$ precursor (navy curve, Fig. 2) and exhibited only one broad peak at $2\theta$=25.9°. As the proportion of water was increased, XRD patterns revealed diffraction peaks corresponding to HAP (JCPDS No. 09-0432) and DCPA (JCPDS No. 09-0080). The relative fraction (F) of HAP and DCPA in products was determined semi-quantitatively from XRD patterns using the empirical formula (Eq. (1)) and the relative ratios of the integrated intensity of the HAP (211) reflection at $2\theta$=31.8° ($I_{HAP}$) and the DCPA (002) reflection at $2\theta$=26.4° ($I_{DCPA}$) [28].

$$F(\%) = \frac{I}{\sum_{phase} I} \times 100 = \frac{I}{I_{HAP} + I_{DCPA}} \times 100 \quad (1)$$

As the proportion of ethanol was increased, HAP fractions gradually decreased from ~100% ($H_2O$/EtOH=100/0) to ~52% (75/25), ~36% (50/50), and ~23% (25/75) and DCPA fractions increased from ~0% (100/0) to ~48% (75/25), ~64% (50/50) and ~77% (25/75).

Note that the XRD pattern (Fig. 2(a) red curve) of the CaP products produced in 100% water matched the reference HAP pattern (JCPDS No. 09-0432). The integrated intensity of the HAP (002) reflection at $2\theta$=25.9° as a percentage of that of the (211) reflection at $2\theta$=31.8° in the reference XRD pattern of HAP (black curve, Fig. 2(a)) was ~40%. However, in the present study, it was slightly higher for the CaP product in 100% water at ~63% (red curve, Fig. 2(a)), which suggested the CaP product produced in 100% water had a rod-like shape elongated along its preferential growth direction. It has been reported that HAP synthesized in aqueous environments exhibits anisotropic rod-like morphologies due to their preferential growth along *c*-axis while obeying their intrinsic crystal habit [29]. This anisotropic growth in the [001] direction is typically accompanied by an increase in exposed (001) and its equivalent faces, which was probably increased the (002) to (211) reflection intensity ratio [30].

FESEM and TEM micrographs of the as-synthesized CaP products synthesized in 100% water confirmed their anisotropic rod-like structures. Figs. 3(a) and (b) show rod-shaped HAP nanostructures that were produced from the $CaIP_6$ nanoparticle precursor under hydrothermal conditions at 180 °C with relatively uniform lengths and widths (111±24 and 28±2 nm, respectively). Selected area of electron diffraction (SAED) patterns of the rod-shaped HAP nanostructures (see Fig. S1 of the supplementary information) demonstrated that they were highly crystalline. The *d*-spacings calculated from SAED patterns were ~0.34, ~0.29, and ~0.26 nm, which were putatively attributed to (002), (211), and (202) or (300) planes, respectively. These results were indeed in good agreement with the XRD results (Fig. 2(a)).

Figs. 3C and D show HRTEM images of these rod-shaped HAP nanostructures. A number of the rod-shaped HAP nanostructures revealed nearly identical lattice fringe highlighted in Fig. 3C. The spacing of the fringe was measured to be 0.343 nm, which corresponds to that of (002) lattice plane [31]. Fig. 3D illustrates two lattice planes with an angle of ~36.1°, which were assigned to the (002) and (112) planes based on measured *d*-spacings of 0.343 and 0.278

**Table 1. Summary of the phases and morphologies of nanostructured calcium phosphate (CaP) products synthesized in water-ethanol mixtures under solvo-hydrothermal conditions**

| $H_2O$/EtOH (% (v/v)) | Phase of CaP | Morphology of CaP |
|---|---|---|
| 100/0 | HAP | Nanorods |
| 75/25 | HAP-rich (HAP-DCPA mixed) | (major) Microspheres composed of rod- and plate-shaped CaP nanostructures (minor) Microrods |
| 50/50 | HAP-DCPA mixed | |
| 25/75 | DCPA-rich (HAP-DCPA mixed) | (major) Micorspheres composed of rod- and plate-shaped CaP nanostructures (minor) Microrods |
| 0/100 | $CaIP_6$ precursor | Aggregated amorphous nanoparticles |

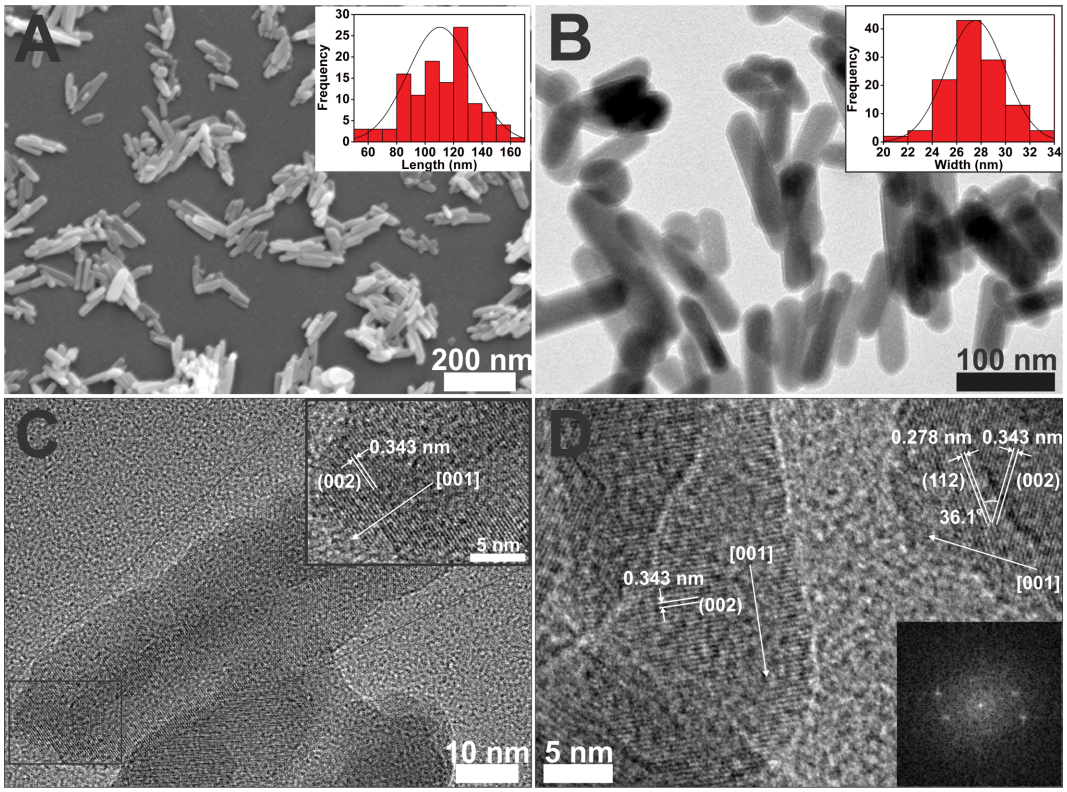



**Fig. 3. (A) FESEM and (B) TEM images of rod-shaped CaP nanostructures synthesized in 100% water solution. Inset plots in Figs. 3A and B show histograms of measured lengths (mean length 111±24 nm) and widths (mean width 28±2 nm) based on 117 counts. (C) and (D) HRTEM images of rod-shaped CaP nanostructures. Two lattice spacings of 0.343 and 0.278 nm were assigned to distances between the (002) and (112) planes of HAP. The inset image in Fig. 3D is the corresponding fast Fourier transform image of the HRTEM lattice fringe images. Based on the analysis performed, rod-shaped CaP nanostructures grew in the [001] direction.**

nm, respectively. Overall, our results indicated that rod-shaped HAP nanostructures typically grew in the [001] direction, which aligned with the *c*-axis of HAP crystals. This is also consistent with the increased ratio of the integrated XRD intensities (red curve, Fig. 2(a)).

Fig. 4 shows the FT-IR spectra of the as-synthesized CaP products synthesized during solvo-hydrothermal conditions. The FT-IR spectrum of $CaIP_6$ precursor (navy curve) exhibited the two characteristic groups of IR bands at ~794, ~840, ~895, ~994 $cm^{-1}$ (C-O-P collective vibrations of the $IP_6$ moiety) and at ~1,130, ~542 $cm^{-1}$ ($PO_4^{2-}$ vibrations of the $IP_6$ moiety) [32]. The FT-IR spectrum of the CaP product (olive curve with $H_2O$/EtOH=0/100) produced using 100% ethanol closely resembled that of the $CaIP_6$ precursor nanoparticle, which suggests the $CaIP_6$ precursor was unchanged. However, the FT-IR spectra of the product (red curve with $H_2O$/EtOH= 100/0) produced in 100% water showed the following characteristic IR bands at ~1,096, ~1,030, ~963, ~634, ~604, and ~563 $cm^{-1}$, which were assigned to the vibration modes of the phosphate ($PO_4^{3-}$) group of the rod-shaped HAP nanostructures. These values are reasonably consistent with reported values of ~1,093 and ~1,030 $cm^{-1}$ ($PO_4^{3-}$ $\nu 3$ bending vibrations of HAP) and ~606 and ~561 $cm^{-1}$ ($PO_4^{3-}$ $\nu 4$ bending vibrations of HAP), respectively [26,33]. Based on the results from elemental analysis (±0.03), the rod-shaped HAP nanostructures produced from $CaIP_6$ precursor in 100% water consisted of a Ca to P atomic ratio of ~1.67 : 1 that corresponds to stoichiometric HAP ($Ca_{10}(PO_4)_6(OH)_2$). Besides, the rod-shaped HAP nanostructures did not exhibit IR bands at 870-880 $cm^{-1}$ that are characteristic of $(HPO_4)^{2-}$ groups present in Ca-deficient HAP ($Ca_{10-x}(HPO_4)_x(PO_4)_{6-x}(OH)_{2-x}$). These results are reasonably consistent with the SAED and HRTEM analyses.

The FT-IR spectra of the products (blue, orange, and magenta curves) in the water-ethanol mixtures showed the following additional characteristic IR bands at ~1,130, ~1,064, and ~902 $cm^{-1}$, which were attributed to the vibration modes of $PO_4^{3-}$ groups of DCPA nanostructures. Furthermore, these values agreed well with reported values of ~1,130, ~1,065, and ~892 $cm^{-1}$ for the vibration modes of $PO_4^{3-}$ groups present in DCPA [15]. Therefore, both XRD and FT-IR analysis confirmed that only the HAP and DCPA phases of the CaP were produced in water-ethanol mixtures.

Table 1 summarizes the phases and morphologies of the CaP products synthesized under solvo-hydrothermal conditions. Fig. 5 shows FESEM micrographs of the as-synthesized CaP products synthesized in the presence of ethanol. When the $CaIP_6$ precursor was solvo-hydrothermally treated in 100% ethanol ($H_2O$/EtOH=0/100), the CaP products remained as amorphous $CaIP_6$ nanoparticles (Fig. 5A and A1). However, as the amount of water was increased ($H_2O$/EtOH=25/75 (Fig. 5B and B1), 50/50 (Fig. 5C and C1), or 75/25 (Fig. 5D and D1)), we made the following observations.

First, nanostructured CaP products aggregated to form microspherical superstructures with uniform diameters in the sub-μm (Fig. 5B) to tens of μm range (Figs. 5C and D) in the $H_2O$/EtOH

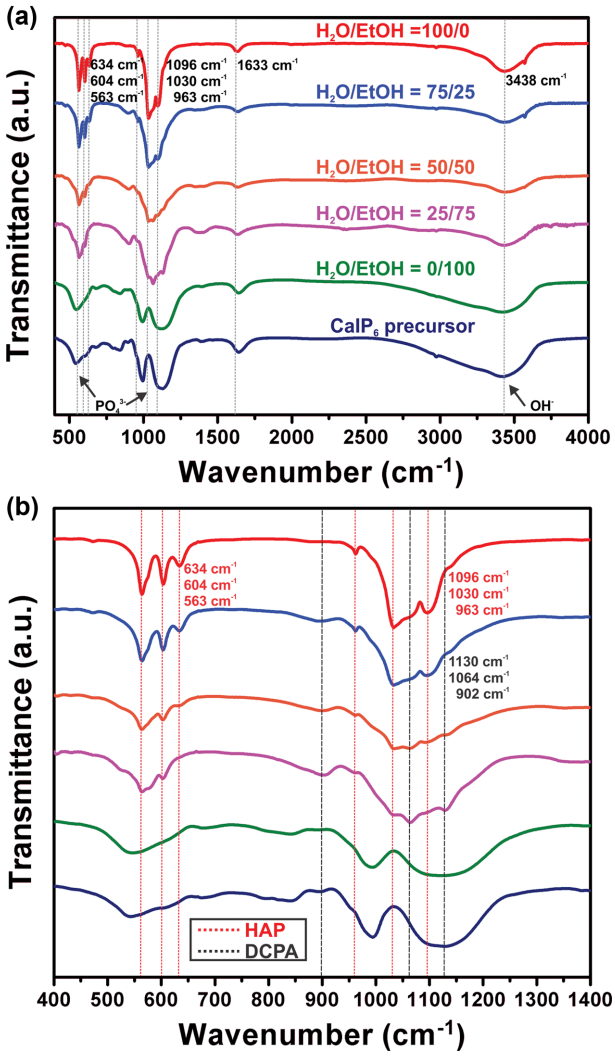



**Fig. 4. (a) Survey FT-IR spectra of CaP nanostructures synthesized in water-ethanol mixtures $H_2O$/EtOH (v/v %)=100/0, 75/25, 50/50, 25/75, and 0/100. Dotted lines indicate peak assignments. (b) Selected regions of the FT-IR spectra of CaP nanostructures synthesized in water-ethanol mixtures $H_2O$/EtOH (v/v %)=100/0, 75/25, 50/50, 25/75, and 0/100. Characteristic IR bands of HAP and DCPA are indicated by red and blue dotted guidelines for comparison.**

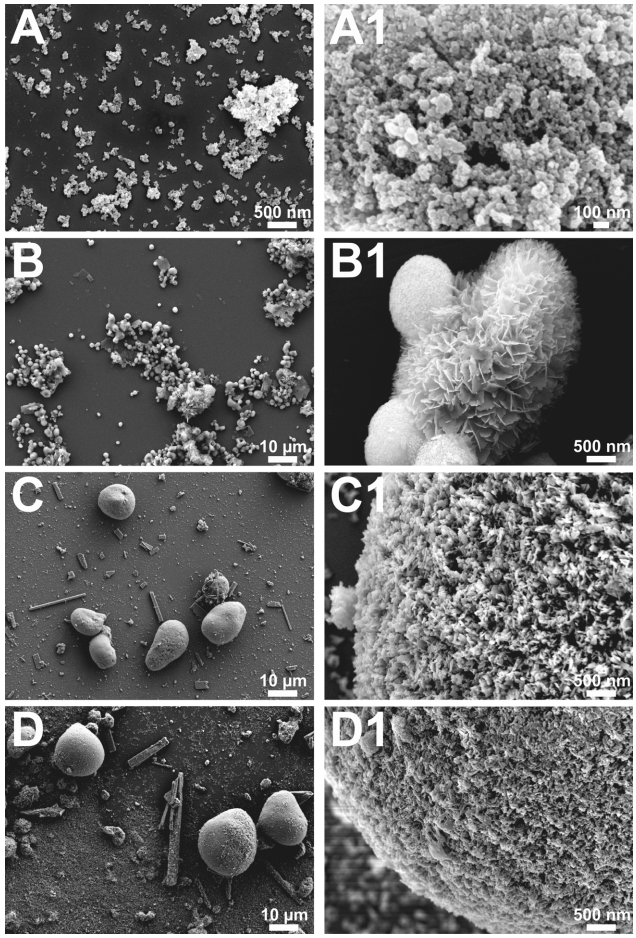



**Fig. 5. (Left column) FESEM images of CaP nanostructures synthesized in water-ethanol mixtures $H_2O$/EtOH (v/v %)=(A) 0/100, (B) 25/75, (C) 50/50, and (D) 75/25. (Right column) high magnification FESEM images of these nanostructures synthesized in water-ethanol mixtures $H_2O$/EtOH (v/v %)=(A1) 0/100, (B1) 25/75, (C1) 50/50, and (D1) 75/25.**

(25/75) mixture. Second, a few different types of microspherical superstructures were produced at $H_2O$/EtOH=25/75 (Figs. 5B and B1), 50/50 (Figs. 5C and C1), and 75/25 (Figs. 5D and D1). One of these types was composed of aggregated $CaIP_6$ precursor nanoparticles and the other predominantly of rectangular plate-shaped CaP nanostructures in the $H_2O$/EtOH (25/75) mixture. However, both rectangular plate- and rod-shaped CaP nanostructures aggregated into microspherical superstructures (Figs. 5C1 and D1) at $H_2O$/EtOH=50/50 and 75/25. Third, microrods of uniform length (30.8±2.9 μm) and width (9.9±1.6 μm) were also produced in $H_2O$/EtOH (50/55) and (75/25) mixture (Figs. 5C and D).

Our FESEM results indicated that the rod- and rectangular plate-shaped CaP nanostructures by solvo-hydrothermal treatments of $CaIP_6$ precursor were composed of HAP and DCPA, and that their phase compositions affected by the relative ratio of water to ethanol. The existence of HAP and DCPA phases and their relative fractions in CaP as determined by FESEM were consistent with the above-mentioned XRD and FT-IR measurements.

Interestingly, $CaIP_6$ nanoparticles were not transformed to HAP or DCPA in 100% ethanol, possibly because of a lack of water required to generate phosphate ions from hydrolysis of $CaIP_6$. It has been reported HAP is the thermodynamically stable phase if $Ca^{2+}$ and $PO_4^{3-}$ ions are reacted hydrothermally at 100 to 200 °C [34]. However, we found that the DCPA to HAP ratio increased with an increase of ethanol concentration in solution. We believe this may be because polarity of the reaction environment plays an important role in determining the phase of CaP nanostructures. Based on the dielectric constants of water and ethanol at 25 °C, which are 78.5 and 24.3, respectively, the dielectric constant of the water-ethanol solutions would decrease as the proportion of ethanol is increased and it would appear that this less polar environment militates against HAP crystal formation [35]. It is also possible that small pH decreases may promote DCPA formation. As has been previ-

ously reported, a slight pH reduction occurs when water is added to aqueous solutions containing a high percentage of ethanol [36]. This increase in $H^+$ ion concentration would result in a shift of the equilibrium between $PO_4^{3-}$ and $HPO_4^{2-}$ ions towards an increase in $HPO_4^{2-}$, hence promoting the formation of DCPA. In fact, the solubilities of all CaPs rapidly increase when pH is reduced, but the rate of increase is highly dependent on the type of CaP. The pH-dependence of the solubility of HAP is greater than that of DPCA, and at a pH values of ≤5.5 the solubility of HAP exceeds that of DCPA; thus, in this acidic range DCPA becomes the more stable phase and its formation is facilitated [37].

Why the rectangular plate- and rod-shaped CaP nanostructures aggregated more to form the microspherical superstructures of uniform diameter and morphology in the water-ethanol solutions is uncertain. One possible explanation is that lowering the overall dielectric constant of the water-ethanol may have boosted interactions between rectangular plate- and rod-shaped CaP nanostructures and caused them to aggregate. This rationalization suggests that the composition of the water-ethanol solutions is an important parameter, which by extension suggests that ethanol content influences the assembly of CaP nanostructures and, consequently, the hierarchical structures of microspheres.

## CONCLUSIONS

We prepared CaP nanostructures from $CaIP_6$ nanoparticles in the water-ethanol solutions using a solvo-hydrothermal method. FESEM, TEM, HRTEM, XRD, and FT-IR analyses of their structures indicated that all products were highly crystalline CaP nanostructures with distinctive shapes and morphologies. Anisotropic rod-shaped CaP nanostructures of relatively uniform length and width were obtained exclusively by the decomposition of $CaIP_6$ in 100% water; these nanostructures had pristine crystal structures with less grain boundary and their crystalline structure equaled to HAP phase. When the same reaction was carried out in the water-ethanol solutions, rod-shaped and rectangular plate-shaped CaP nanostructures were both produced. The ratios of HAP to DCPA phases in these nanostructure were influenced by the water to ethanol ratio that seemed to dictate the solution polarity. As the ethanol fraction increased, the formation of HAP-rich rod-shaped CaP nanostructures gave way to the formation of DCPA-rich rectangular plate-shaped CaP nanostructures. Our findings are significant because they enable control of the size, morphology, and crystalline structures of CaP nanostructures. Consequently, we believe the described method can be utilized to improve morphological control of novel biomaterials for bone regeneration and repair applications.

## ACKNOWLEDGEMENTS

This work was supported by the Basic Science Research Program through the National Research Foundation of Korea (NRF), funded by the Ministry of Education, Korea (NRF-2015R1D1A1A01059580 and NRF-2019R1F1A1060060), by the Nano-Material Technology Development Program through the National Research Foundation of Korea (NRF) funded by the Ministry of Science, ICT and Future Planning (2009-0082580), and by the Basic Core Technology Development Program for the Oceans and the Polar Regions of the National Research Foundation of Korea (NRF) funded by the Ministry of Science and ICT (NRF-2015M1A5A1037054).

## SUPPORTING INFORMATION

Additional information as noted in the text. This information is available via the Internet at http://www.springer.com/chemistry/journal/11814.

## REFERENCES

1. C. Combes, S. Cazalbou and C. Rey, *Minerals*, **6**, 34 (2016).
2. S. V. Dorozhkin, *Materials*, **6**, 3840 (2013).
3. M. Epple, K. Ganesan, R. Heumann, J. Klesing, A. Kovtun, S. Neumann and V. Sokolova, *J. Mater. Chem.*, **20**, 18 (2010).
4. W. Habraken, P. Habibovic, M. Epple and M. Bohner, *Mater. Today*, **19**, 69 (2016).
5. Y. Q. Shen, Y. J. Zhu, F. F. Chen, Y. Y. Jiang, Z. C. Xiong and F. Chen, *J. Mater. Chem. B*, **6**, 4985 (2018).
6. J. Zhao, Y. Liu, W. B. Sun and H. Zhang, *Chem. Cent. J.*, **5**, 1 (2011).
7. M. Nagano, T. Nakamura, T. Kokubo, M. Tanahashi and M. Ogawa, *Biomaterials*, **17**, 1771 (1996).
8. R. A. Surmenev, M. A. Surmeneva and A. A. Ivanova, *Acta Biomater.*, **10**, 557 (2014).
9. R. Mi, Y. Liu, X. Chen and Z. Shao, *Nanoscale*, **8**, 20096 (2016).
10. S. Bose and S. Tarafder, *Acta Biomater.*, **8**, 1401 (2012).
11. K. W. Wang, Y. J. Zhu, X. Y. Chen, W. Y. Zhai, Q. Wang, F. Chen, J. A. Chang and Y. R. Duan, *Chem. Asian J.*, **5**, 2477 (2010).
12. L. X. Yang, J. J. Yin, L. L. Wang, G. X. Xing, P. Yin and Q. W. Liu, *Ceram. Int.*, **38**, 495 (2012).
13. J. M. Delgado-Lopez, M. Iafisco, I. Rodriguez-Ruiz and J. Gomez-Morales, *J. Inorg. Biochem.*, **127**, 261 (2013).
14. K. L. Lin, C. T. Wu and J. Chang, *Acta Biomater.*, **10**, 4071 (2014).
15. M. Sadat-Shojai, M. T. Khorasani and A. Jamshidi, *J. Cryst. Growth*, **361**, 73 (2012).
16. H. Ito, Y. Oaki and H. Imai, *Cryst. Growth Des.*, **8**, 1055 (2008).
17. Y. Y. Jiang, Y. J. Zhu, F. Chen and J. Wu, *Ceram. Int.*, **41**, 6098 (2015).
18. N. Eliaz and N. Metoki, *Materials*, **10**, 334 (2017).
19. A. Haider, S. Haider, S. S. Han and I. K. Kang, *RSC Adv.*, **7**, 7442 (2017).
20. A. Fihri, C. Len, R. S. Varma and A. Solhy, *Coord. Chem. Rev.*, **347**, 48 (2017).
21. A. C. Tas, *J. Am. Ceram. Soc.*, **92**, 2907 (2009).
22. Y. R. Cai and R. K. Tang, *J. Mater. Chem.*, **18**, 3775 (2008).
23. D. Q. Xiao, Z. Tan, Y. K. Fu, K. Duan, X. T. Zheng, X. Lu and J. Weng, *Ceram. Int.*, **40**, 10183 (2014).
24. A. Shamsuddin and J. von Fraunhofer, US Pattern Application Publication, US 2007/0212449 A1 (2007).
25. F. Grases, M. Ramis and A. Costa-Bauzá, *Urol. Res.*, **28**, 136 (2000).
26. D. Q. Xiao, F. Yang, X. Zhou, Z. Chen, K. Duan, J. Weng and G. Feng, *RSC Adv.*, **7**, 44371 (2017).
27. Z. Q. He, C. W. Honeycutt, T. Q Zhang and P. M. Bertsch, *J. Environ. Qual.*, **35**, 1319 (2006).
28. T. Goto, I. Y. Kim, K. Kikuta and C. Ohtsuki, *Ceram. Int.*, **38**, 1003 (2012).

29. L. J. Hao, H. Yang, S. L. Du, N. R. Zhao and Y. J. Wang, *Mater. Lett.*, **131**, 252 (2014).
30. M. Dardouri, J. P. Borges and A. D. Omrani, *Ceram. Int.*, **43**, 3784 (2017).
31. R. X. Sun, L. L. Yang, Y. X. Zhang, F. Chu, G. Y. Wang, Y. P. Lv and K. Z. Chen, *CrystEngComm*, **18**, 8030 (2016).
32. K. Ganesan and M. Epple, *New J. Chem.*, **32**, 1326 (2008).
33. J. H. Han and S. Chung, *Appl. Chem. Eng.*, **29**, 740 (2018).
34. M. Yoshimura, P. Sujaridworakun, F. Koh, T. Fujiwara, D. Pongkao and A. Ahniyaz, *Mater. Sci. Eng. C*, **24**, 521 (2004).
35. M. J. Larsen, A. Thorsen and S. J. Jensen, *Calcified Tissue Int.*, **37**, 189 (1985).
36. W. Gelsema, C. De Ligny, A. Remijnse and H. Blijleven, *Recueil. des. Travaux. Chimiques. Des. Pays.*, **85**, 647 (1966).
37. X. Y. Liu, *Bioinspiration: from nano to micro scales*, Springer, New York (2012).

# Supporting Information

# Solvo-hydrothermal synthesis of calcium phosphate nanostructures from calcium inositol hexakisphosphate precursor in water-ethanol mixed solutions

**Ji-Hoon Han*, Seung Pil Pack**, and Sungwook Chung*,†**

*School of Chemical and Biomolecular Engineering, Pusan National University,
2 Busandaehak-ro 63beon-gil, Geumjeong-gu, Busan 46241, Korea
**Department of Biotechnology and Bioinformatics, Korea University, 2511 Sejong-ro, Sejong 30019, Korea
(*Received 30 September 2019 • accepted 18 January 2020*)

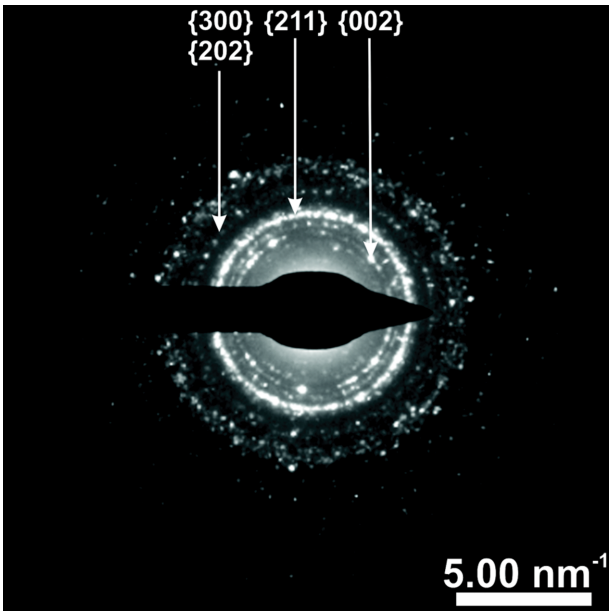



**Fig. S1. Selected area electron diffraction (SAED) pattern of as-synthesized rod-shaped CaP nanostructures in the pure water solution. The diffraction pattern shows several ring patterns composed of bright spots that are indexed to the set of {300} and {202}, {211}, and {002} equivalent planes belong to the hexagonal lattice of HAP.**